Hierarchical SnO_2 Nanostructures: Linear Assembly of Nanorods on the Nanowire Backbones

Hongxing Li,[†] Haiqing Ma,[†] Yaping Zeng,[†] Anlian Pan,[†] Qinglin Zhang,[†] Hongchun Yu,[†] Taihong Wang,[†] Yanguo Wang,*[,†,‡] and Bingsuo Zou*[,†]

Micro-Nano Technologies Research Center, Key Lab for Micro-Nano Optoeletronic Devices of MOC, Hunan University, Changsha 410082, China, and Institute of Physics, Chinese Academy of Sciences, P.O. Box 603, Beijing 100080, China

Received: December 4, 2009

Single-crystalline SnO_2 nanorods were successfully assembled on SnO_2 nanowire backbones through a sequential gold-catalyzed thermal evaporation method. Scanning electron microscopy (SEM) and transmission electron microscopy (TEM) studies showed that uniform secondary nanorod branches were epitaxially grown from two side surfaces of the nanowire backbones. These branch rods are parallel to each other with 2-fold symmetry with respect to the backbones. The crystal structure of these as-prepared SnO_2 centipede-like nanostructures was identified to coincide to the normal rutile structure. The photoluminescence (PL) properties of single centipede-like SnO_2 structures were studied by confocal microscopy, which showed that these structures can act as good optical waveguides. Cathodoluminescence (CL) spectra of the SnO_2 branched structures obtained in the SEM−CL system featured a blue emission band around 462 nm that is attributed to a defect-state-related emission.

Introduction

Nanostructured materials with controllable size and morphology have been the focus of intensive research in recent years, because such materials are very important in the development of highly integrated and small-size devices. Hierarchical assembly of nanoscale building blocks is a crucial step toward the realization of functional nanosystems in the field of nanoscale science.[1−4] Recently, significant advances have been made in the fabrication of three-dimensionally hierarchical nanostructures. For example, branched, flower-like, and tetrapod-shaped nanostructures have been fabricated by thermal evaporation or chemical vapor deposition (CVD) routes.[1,2,5−9] However, the fabrication of ordered three-dimensionally hierarchical nanostructures is still a challenge. The ability to control the size, dimensions, and composition of building blocks of hierarchical nanostructures in a predictable manner is still highly desired for the realization of multifunctional nanodevices.

SnO_2 is an important n-type metal oxide semiconductor with a wide band gap (E_g = 3.6 eV at 300 K). As a transparent conducting oxide (TCO), it has a long history of use as an electronic conductor. Recently, dramatic progress has been made in the synthesis of SnO_2 quasi-one-dimensional (Q1D) nanostructures, such as nanowires,[10] nanorods,[11] and nanobelts,[12,13] which have been used extensively in optoelectronic devices[14] and gas sensors for detecting leakages of reducing gases such as NO_2[15,16] and CO.[17] A variety of branched SnO_2 nanostructures have also been prepared through noncatalytic[18,19] and Sn-particle-assistant self-catalytic[20] growth mechanism. However, these products are ragged in morphology because of the noncontrollable growth process, which limits their further applications. Because the properties of hierarchical systems are greatly influenced by their morphologies, sizes, and orientations, controllable synthesis of orderly assembled junction arrays of SnO_2 are desirable for achieving unique functionalities and offering integrated three-dimensional structures for nanowire-based device design.[7] In this article, we report a technique for the linear assembly of single-crystal SnO_2 nanorods on pregrown SnO_2 nanowire backbones by a sequential Au-catalyzed thermal evaporation route. The obtained hierarchical structures are 2-fold symmetrical, with their branches parallel to each other and perpendicular to the nanowire backbones. Optical measurements show that the prepared centipede-like structures are still good waveguide cavities. Cathodoluminescence (CL) analysis was used to determine the crystalline quality and the presence of defect structures in the branched nanostructures, in which a broad white-blue luminescence ranging from 350 to 600 nm was revealed. This type of SnO_2 hierarchical nanostructure might have potential applications in field-effect transistors (FETs), solar cells, and gas sensors.

Experiments

Centipede-like SnO_2 hierarchical nanostructures were synthesized through a two-step Au-catalyzed thermal evaporation route. Briefly, Sn powder (1 g, 99.9%) was loaded in a ceramic boat that was covered with one piece of Si wafer. Ten-nanometer-thick Au film was predeposited on the Si wafer to serve as the catalysts for the growth of ultralong SnO_2 nanowire backbones. The perpendicular distance between the Si wafer and the Sn powder was 5 mm. The boat was positioned in a quartz tube that was inserted into a horizontal tube furnace. High-purity Ar (99.999%) was flowed into the quartz tube to adjust the oxygen pressure in the tube. Then, the furnace was heated to 900 °C and held at this temperature for 90 min. After the furnace cooled to room temperature, a thin layer of white wool-like products formed on the Si substrate. For the growth of the highly ordered nanorod branches, a 3-nm layer of Au was deposited on the obtained SnO_2 nanowires and annealed at

* To whom correspondence should be addressed. E-mail: ygwang@blem.ac.cn (Y.W.), bszou@hnu.cn (B.Z.).
† Hunan University.
‡ Chinese Academy of Sciences.

10.1021/jp911514t
Published on Web 01/07/2010

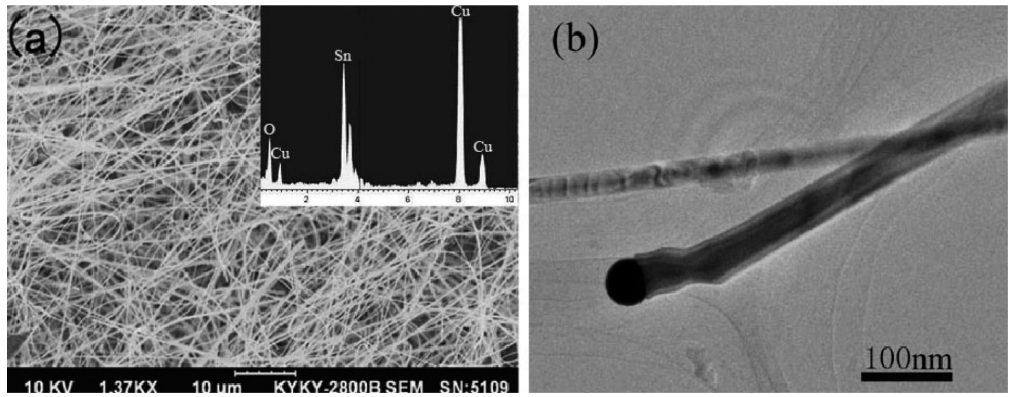

Figure 1. (a) SEM and (b) TEM images of the SnO_2 nanowire backbones at low magnification. The inset in a is the corresponding EDS spectrum, showing the Sn and O atomic ratio of approximately 1:2.

600 °C in Ar ambient for 30 min. The Au-decorated SnO_2 nanowires then served as backbones for the subsequent branched nanorod assembly. The growth time for the branches was 10 min with the other growth conditions the same as for the backbones.

The morphologies and microstructures of the as-prepared products were characterized and analyzed by field-emission scanning electron microscope (FE-SEM, model JSM-6700F), X-ray diffractometer (XRD, model MXPAHF), and high-resolution transmission electron microscope (HRTEM, model 3010) operated at 300 kV. Their compositions were measured by energy-dispersive X-ray spectroscopy (EDS) attachments on the electron microscopes. Raman spectra were obtained by near-field scanning optical microscope (NSOM) excited by an Ar^+ laser (488 nm) at room temperature. The PL of single centipede-like SnO_2 nanostructures was detected at room temperature using a He−Cd laser (325 nm) as the excitation source. An Oxford Mono CL apparatus equipped for SEM was used for CL spectroscopy. The accelerating voltage for this study was varied from 10 to 30 kV. The CL spectrum of the hierarchical SnO_2 nanostructure was obtained by scanning the electron beam over an area of 10 μm × 10 μm at room temperature.

Results and Discussion

The bare nanowires without branches were first observed by FE-SEM and TEM. As shown in Figure 1a, these nanowires were uniformly distributed on the Si substrate, with diameters of 50−400 nm and lengths of up to several tens of micrometers. Figure 1b is a low-magnification TEM image of two typical nanowires, which confirms that they are very uniform in size and have a smooth surface. A Au nanoparticle with dark contrast can also be seen at the tip of the nanowires. The HRTEM image shown in Figure 2 indicates that these SnO_2 wires are high-quality single crystals. The interplanar spacing of ~0.47 nm corresponds to the distance of the neighboring (100) planes in tetragonal rutile SnO_2. The corresponding fast Fourier transform (FFT) is shown in the upper-right inset of Figure 2, which can be well-indexed for the [010] zone axis of tetragonal SnO_2. Thus, these single-crystalline SnO_2 wires have a preferential growth direction along the *a* axis, the [100] crystal direction. The EDS pattern taken on the nanowire shows the presence of only the two elements Sn and O, with a rough atomic ratio of about 1:2 (the Cu peak originates from the copper grid).

The crystal structure of the as-grown nanowires was determined by XRD. All of the diffraction peaks shown in Figure 3a can be perfectly indexed based on the tetragonal rutile SnO_2 structure with lattice constants of $a = b = 0.47$ nm and

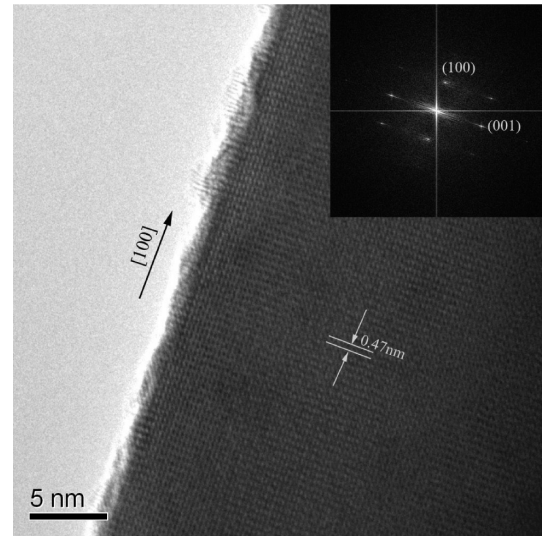

Figure 2. Typical HRTEM image of a single SnO_2 nanowire backbone along the [010] zone axis. The inset shows the Fourier transform of the HRTEM image.

$c = 0.32$ nm listed in the standard data file (JCPDS file no. 77-0450). The enhanced (200) reflection suggests that the SnO_2 nanowires grew preferentially along the [100] direction, which is consistent with the results of TEM examination. The rutile characteristics of these SnO_2 nanowires were further confirmed by the Raman spectrum measurement. As shown in Figure 3b, the spectrum has a good signal-to-noise ratio, and the peaks located at 477, 636, and 776 cm^{-1} are attributed to the E_g, A_{1g}, and B_{2g} phonon modes, respectively, of rutile SnO_2.[21]

Parts a and b of Figure 4 show the representative morphologies of the obtained hierarchical nanowire structures after the growth of branches on the preprepared nanowire backbones by two-step growth. The branched nanorods are assembled on the two side faces of the nanowire backbones and are parallel to each other. The distance between two neighboring branches ranges from 50 to 100 nm, resulting in the centipede-like morphology shown in Figure 4b. The size of the branches on a single backbone is very uniform, with a length of ~900 nm.

Further microstructural analysis of the branched nanostructures was performed by TEM. The TEM image of the branched nanostructures in Figure 5a shows a typical centipede-like morphology. The Au nanoparticles are clearly seen at the tips of the branches, with a size only slightly larger than the diameter of the branch nanowires. A sharp interface is clearly shown between the catalyst and the SnO_2 nanorod along the growth direction (Figure 5b), resulting in very straight branches. An

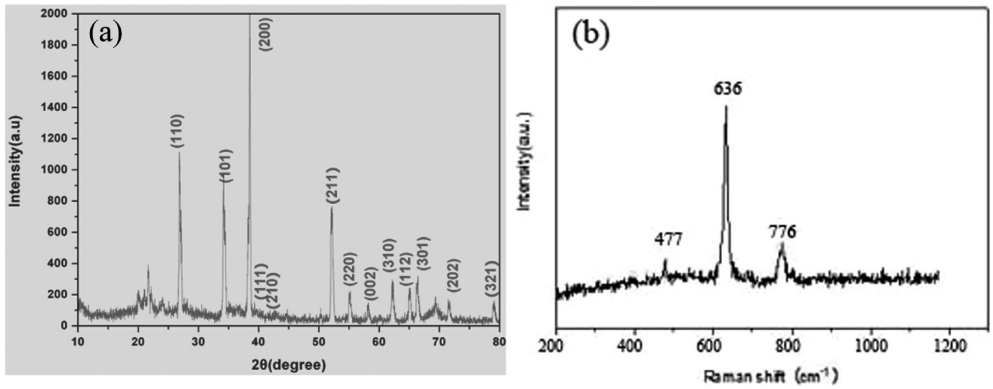

Figure 3. (a) X-ray diffraction patterns and (b) room-temperature Raman spectra of the SnO_2 nanowires.

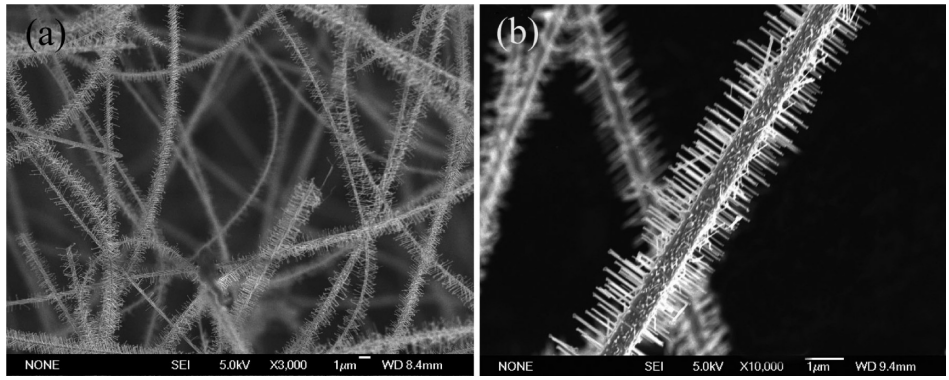

Figure 4. SEM images showing the major characteristics of the as-synthesized SnO_2 hierarchical nanostructures: (a) branched structures at low magnification and (b) centipede-like morphology at high magnification.

interesting feature revealed in the TEM image of Figure 5a is that all of the branches are perpendicular to the backbone nanowires. In addition to the Au particles at the tips of the branched nanorods grown on the two symmetric side surfaces of the backbone, Au particles also remained on the other two side surfaces without branch growth, as marked by the circles in Figure 5a. Figure 5c shows the HRTEM image observed from the stem of the nanorod branches. The lattice constant perpendicular to the growth direction of the branches is 0.47 nm (at the bottom left corner), corresponding to the (010) or (100) planes of rutile SnO_2. This value is also equal to the (100) lattice plane parallel to the backbone nanowire growth direction, indicating that the branches are epitaxially grown from the backbones. The corresponding selected-area electron diffraction (SAED) pattern inserted at the top right corner of Figure 5c can be well-indexed based on rutile SnO_2, and the nanorod branch is easily determined to be grown along the [001] direction, consistent with the results reported by Zhao et al.[22] Figure 5d is an HRTEM image of the junction region, where the crystalline structure of the branch can be obviously found to continue into the backbone without breaking, further showing a perfect epitaxial growth of the branch on the backbone. Such branched nanowires are highly desirable for the improvement of the performance of nanowire-based sensors[23,24] and photovoltaic devices[25] owing to the increased interface and surface area in the structures.

Branched SnO_2 nanostructures with their branches grown perpendicularly to the backbone have also been reported recently, such as self-catalyst growth of fishbone-like nanostructures with branches along the [301] lattice orientation[26] and SnO_2 nanowire arrays with the [001] direction formed on the two crude surfaces of primary quasihexagonal microds.[27] However, the centipede-like SnO_2 nanostructures revealed in this work have a different configuration, with the backbone and branches along the [100] and [001] directions, respectively.

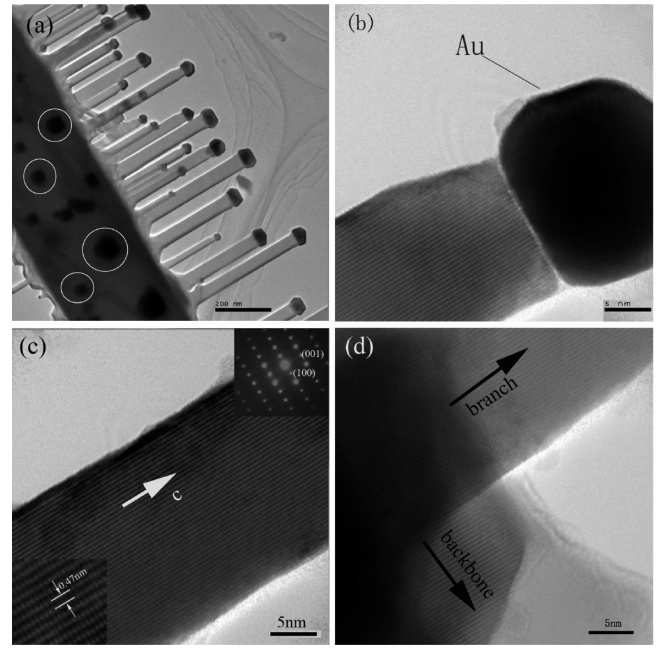

Figure 5. (a) Typical TEM image of the centipede-like SnO_2 branched nanostructure show the macroscopic 2-fold morphology. (b) HRTEM image showing an individual nanorod branch terminated with a Au nanoparticle. (c) HRTEM image of the stem of a nanorod branch showing the crystal structure in detail. The inset at the right top is the corresponding SAED pattern obtained from the branch region, and the inset at the left bottom is the corresponding highly magnified HRTEM image. (d) HRTEM image showing the junction of a typical branched nanostructure.

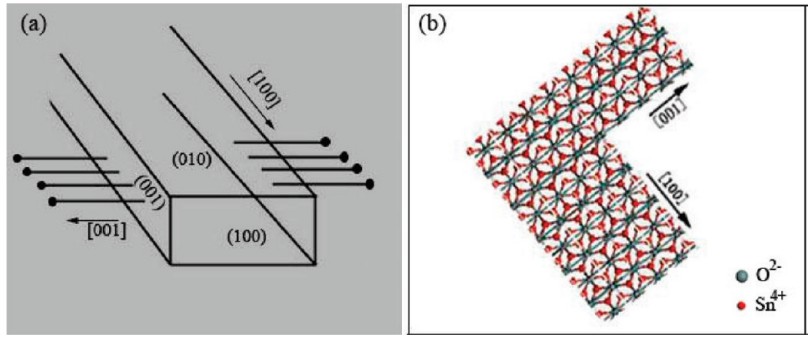

Figure 6. Schematic diagrams of (a) the alignment of nanorod branches grown on the side surfaces of the nanowire backbone and (b) the epitaxial relationship between the backbones and branches on an atomic scale from the [010] zone axis.

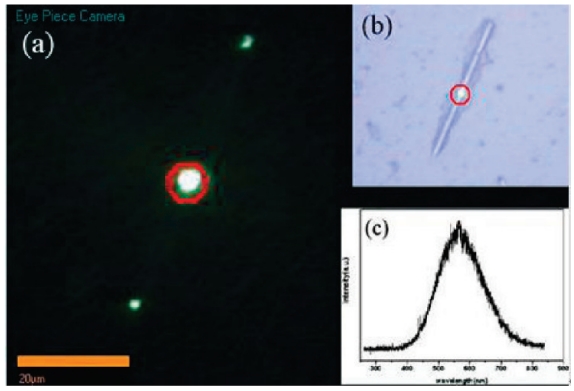

Figure 7. (a) Far-field optical image of an excited linear SnO_2 centipede-like nanostructure showing visble light transport along the backbone nanowire and emission at the ends. (b) Corresponding bright-field topography. (c) Corresponding micro-PL spectrum at room temperature; the red circle is the excitation spot.

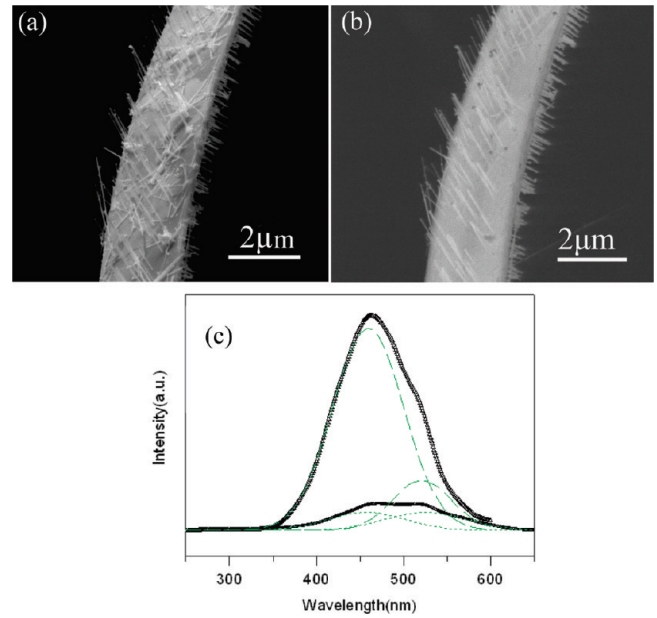

Figure 8. (a) Secondary-electron image and (b) monochromatic CL image. (c) CL spectra of the hierarchical SnO_2 nanostructures under excitation by high- and low-energy electron beams.

The formation of such a structure comes from that the nanorod branches can only grow on the specific crystallographic planes of the SnO_2 backbone nanowires. The vapor−liquid−solid (VLS) growth process provides an elastic boundary condition for the epitaxial growth where liquid alloy droplets are formed by the Au catalyst. The deposition and crystallization of the SnO_2 nanorod takes place from the liquid alloy droplets located at the surface of the backbone that lie in the [100] zone axis. Because SnO_2 nanowires growing along the [100] direction display the {001} and {010} lattice planes as surface facets,[10] the {001} planes, which have higher surface energy than the {010} planes in the backbone, might offer the intrinsic basal floor for this 2-fold-symmetric growth, whereas the {010} planes are suppressed for epitaxial deposition because of their relatively lower surface energy. This point has good consistency with the TEM examinations (Figure 5a), which showed Au particles still attached to the backbone, as well as to the tips of the nanorods.

The orientation relations between the epitaxial branched nanorods and the backbones are shown schematically in Figure 6a. The backbone nanowire with the [100] growth direction has a (010) top surface and {001} side surfaces. Branched nanowires growing on the two {001} side surfaces are perpendicular to the backbone. The epitaxial relationship between the backbone and branches at an atomic scale is well illustrated in Figure 6b, which is shown along the [010] zone axis.

Figure 7a is a far-field PL image of an excited centipede-like SnO_2 nanostructure, and Figure 7b is the corresponding bright-field topography. One can see the centipede-like nanostructures can provide strong visible-light emission, and the emitted light can be transported along their long axes and reflected at their ends. This result indicates that such hierarchical structures can still work as good optical waveguide cavities, similarly to the observations for individual nanowires.[28] However, from the far-field PL image, one cannot see light emission from the radial branches. There are two reasons for this: (i) The length (<900 nm) of these branch rods is too short and near the resolution limit of the CCD optical system. (ii) Most importantly, the diameter (<40 nm; see the TEM image in Figure 5a) of the branches is too small (compared to the visible-light wavelength) to guide the light from the backbone into the branches. Further work based on CL measurements was carried out to determine more emission details of the hierarchical structures (see Figure 8 and the discussion in the next paragraph). Figure 7c shows the corresponding in situ micro-PL spectrum from the excitation spot (see the red circle) at room temperature, which exhibits a broad emission band centered at about 558 nm. As reported, this emission band is caused by oxygen vacancies and other crystal defects formed during the growth.[29−31]

Figure 8c shows the CL spectra under the excitations of high- and low-energy electron beams, respectively, in which a broad asymmetrical white-blue luminescence band ranging from 350 to 600 nm is revealed. The emission intensity was remarkably increased when the acceleration voltage was varied from 10 to 30 kV. Comparison of the secondary-electron image (SE) and the relevant CL images (Figure 8a,b) reveals that both the

backbone and the branches have intense light emission under electron beam excitation, and the emission intensity from the branch nanorod arrays is slightly stronger than that of the thick backbone.

It is worth noting that the near-band-edge (NBE) emission (expected around 320 nm) is not detected in either the PL or CL spectra. This is most probably due to the dipole-forbidden nature of the first transition in semiconductor SnO_2, as reported in the literature.[32,33] Gaussian deconvolution of the CL spectrum shows that both of the visible emission bands consist of two components centering at 460 and 520 nm. Because the deconvolved peak position does not change dramatically with increasing injection power, the peak might be related to defect levels associated with oxygen vacancies or tin interstitials resulting from the nanosized SnO_2. On the other hand, oxygen vacancys (O_V) and tin interstitials (Sn_I) have surprisingly low formation energies and strong mutual attractions;[34] therefore, O_V and Sn_I could form easily with little energetic cost in SnO_2 lattices. The interactions between oxygen vacancies (O_V) and tin interstitials (Sn_I) would lead to the formation of a significant number of trapped states, which would form a series of metastable energy levels within the band gap and result in a strong and broad emission signal at room temperature.[35] By increasing the injection power in O_V-rich or Sn-rich SnO_2 nanostructures, the relative integrated intensities of the different emissions underneath the main CL band change due to the increased concentration of O_V states coming from the interaction between energetic electrons and the lattice.

Conclusion

Centipede-like SnO_2 nanostructures have been prepared in a large scale by a two-step Au-catalyzed thermal evaporation route at 900 °C. The crystallographic epitaxial relationship between the well-aligned nanorods and the nanowire backbone has been demonstrated in detail. The formation mechanism of the structures was thoroughly investigated. Under laser excitation, individual centipede-like structures display a strong green-yellow emission and can still work as good waveguide cavities. CL measurements from the branched nanostructures show a blue emission ranging from 350 to 600 nm depending on the excitation power. No NBE emission is observed, and this blue emission is caused mainly by defect levels associated with oxygen vacancies and tin interstitials. To our understanding, this type of highly assembled structure will hold great promise for applications in FETs, photoelectric converters, and high-sensitivity detectors.

Acknowledgment. The authors are grateful for the financial support of the NSFC of China (Nos. 90606001, 60796078, 60571044, 10774174, 90923014, 10974050, and 20903038), the Hunan Provincial Natural Science Fund for Distinguished Young Scholars (09JJ1009), the Program for New Century Excellent Talents in University (NCET-08-0182), the 973 National Key Basic Research program of MOST of China (2007CB310500, 2007CB936301), and the Open Fund of Key Laboratory of Low Dimensional Quantum Structures and Quantum Control of Ministry of Education (No. QSQC0912).

References and Notes

(1) Dick, K. K.; Deppert, K.; Larsson, M.; Martensson, T.; Seiffert, W.; Wallenberg, L. R.; Samuelson, L. *Nat. Mater.* **2004**, *3*, 380–384.
(2) Jung, Y.; Dong-Kyun Ko, D. K.; Agarwal, R. *Nano Lett.* **2007**, *7*, 264–268.
(3) Pauzauskie, P. J.; Yang, P. *Mater. Today* **2006**, *9*, 36–45.
(4) Guo, S. J.; Wang, L.; Wang, E. K. *Chem. Commun.* **2007**, 3163–3165.
(5) Zhang, Z. X.; Yuan, H. J.; Gao, Y.; Wang, J. X.; Liu, D. F.; Shen, J.; Liu, L. F.; Zhou, W. Y.; Xie, S. S. *Appl. Phys. Lett.* **2007**, *90*, 153116–153118.
(6) Gong, J. F.; Yang, S. G.; Huang, H. B.; Duan, J. H.; Liu, H. W.; Zhao, X. N.; Zhang, R.; Du, Y. W. *Small* **2006**, *2*, 732–735.
(7) Wan, Q.; Dattoli, E. N.; Fung, Y. W.; Guo, W.; Chen, Y. B.; Pan, X. Q.; Lu, W. *Nano Lett.* **2006**, *6*, 2909–2915.
(8) Zhang, F.; Wu, Q.; Wang, X. B.; Liu, N.; Yang, J.; Hu, Y. M.; Yu, L. S.; Wang, X. Z.; Hu, Z.; Zhu, J. M. *J. Phys. Chem. C.* **2009**, *113*, 4053–4058.
(9) Xu, L.; Su, Y.; Li, S.; Chen, Y. Q.; Zhou, Q. T.; Yin, S.; Feng, Y. *J. Phys. Chem. B* **2007**, *111*, 760–766.
(10) Park, M. S.; Wang, G. X.; Kang, Y. M.; Wexler, D.; Dou, S. X.; Liu, H. K. *Angew. Chem., Int. Ed.* **2007**, *46*, 750–753.
(11) Vayssieres, L.; Graetzel, M. *Angew. Chem., Int. Ed.* **2004**, *43*, 3666–3670.
(12) Dai, Z. R.; Gole, J. L.; Stout, J. D.; Wang, Z. L. *J. Phys. Chem. B* **2002**, *106*, 1274–1279.
(13) Dai, Z. R.; Pan, Z. W.; Wang, Z. L. *Solid State Commun.* **2001**, *118*, 351–354.
(14) Mathur, S.; Barth, S.; Shen, H.; Pyun, J. C.; Werner, U. *Small* **2005**, *1*, 713–717.
(15) Kolmakov, A.; Klenov, D. O.; Lilach, Y.; Stemmer, S.; Moskovits, M. *Nano Lett.* **2005**, *5*, 667–673.
(16) Maiti, A.; Rodriguez, A. R.; Law, M.; Kung, P.; McKinney, J. R.; Yang, P. D. *Nano Lett.* **2003**, *3*, 1025–1028.
(17) Yang, M. R.; Chu, S. Y.; Chang, R. C. *Sens. Actuators B* **2007**, *122*, 269–273.
(18) Ra, H. W.; Kim, K. J.; Im, Y. H. *Superlattices Microstruct.* **2008**, *44*, 728–734.
(19) Sun, S. H.; Meng, G. W.; Zhang, G. X.; Masse, J. P.; Zhang, L. D. *Chem.—Eur. J.* **2007**, *13*, 9087–9092.
(20) Chen, Y. X.; Campbell, L. J.; Zhou, W. L. *J. Cryst. Growth* **2004**, *270*, 505–510.
(21) Sun, S. H.; Meng, G. W.; Zhang, G. W.; Gao, G. X.; Geng, T.; Zhang, B. Y.; Zuo, L. D. *Chem. Phys. Lett.* **2003**, *376*, 103–107.
(22) Zhao, J. W.; Ye, C. H.; Fang, X. S.; Qin, L. R.; Zhang, L. D. *Cryst. Growth Des.* **2006**, *6*, 2643–2647.
(23) Patolsky, F.; Zhang, G.; Hayden, O.; Lakadamyali, M.; Zhuang, X.; Lieber, C. M. *Proc. Natl. Acad. Sci. U.S.A* **2004**, *101*, 14017–14022.
(24) Li, C. C.; Li, L. M.; Du, Z. F.; Yu, H. C.; Xaing, Y. Y.; Li, Y.; Cai, Y.; Wang, T. H. *Nanotechnology* **2008**, *19*, 035501−035504.
(25) Huynh, W. U.; Dittmer, J. J.; Alivisatos, A. P. *Science* **2002**, *295*, 2425–2427.
(26) Kim, H. W.; Kim, N. H.; Myung, J. M.; Shim, S. H. *Phys. Status Solidi* **2005**, *202*, 1758–1762.
(27) Liu, J.; Chen, X. L.; Wang, W. J.; Song, B.; Huang, Q. S. *Cryst. Growth Des.* **2009**, *9*, 1757–1761.
(28) (a) Pan, A. L.; Wang, X.; He, P. B.; Zhang, Q. L.; Wan, Q.; Zacharias, M.; Zhu, X.; Zou, B. S. *Nano Lett.* **2007**, *7*, 2970–2975. (b) Pan, A. L.; Liu, D.; Liu, R. B.; Wang, F. F.; Zhu, X.; Zou, B. S. *Small* **2005**, *1*, 980–983. (c) Law, M.; Sirbuly, D.; Johnson, J.; Goldberger, J.; Saykally, R.; Yang, P. *Science* **2004**, *305*, 1269–1273.
(29) Hu, J. Q.; Ma, X. L.; Shang, N. G.; Xie, Z. Y.; Wong, N. B.; Lee, C. S.; Lee, S. T. *J. Phys. Chem. B* **2002**, *106*, 3823–3826.
(30) Luo, S. H.; Fan, J. Y.; Chu, P. K. *Nanotechnology* **2006**, *17*, 1695–1699.
(31) He, J. H.; Wu, T. H.; Wang, Z. L. *Small* **2006**, *1*, 116–120.
(32) Agekyan, V. T. *Phys. Status Solidi A* **1977**, *43*, 11–42.
(33) Zhou, W. C.; Liu, R. B.; Wan, Q.; Zhang, Q. L.; Pan, A. L.; Guo, L.; Zou, B. S. *J. Phys. Chem. C* **2009**, *113*, 1719–1726.
(34) Kilic, C.; Zunger, A. *Phys. Rev. Lett.* **2002**, *88*, 095501−095504.
(35) Her, Y. C.; Wu, J. Y.; Lin, Y. R.; Tsai, S. Y. *Appl. Phys. Lett.* **2006**, *89*, 043115−043118.

JP911514T